AN "AC INDUCTOR" BASED GRID CONNECTED INVERTER

Ilya Zeltser, *Student Member, IEEE* and Sam Ben-Yaakov, *Senior Member, IEEE*

Power Electronics Laboratory
Department of Electrical and Computer Engineering
Ben-Gurion University of the Negev
P.O. Box 653, Beer-Sheva 84105, ISRAEL.
Phone: +972-8-646-1561; Fax: +972-8-647-2949;
Emails: ilyaz@ee.bgu.ac.il, sby@ee.bgu.ac.il; Website: www.ee.bgu.ac.il/~pel

Abstract: **This study proposes a soft switched Output Current Sourcing (OCS) grid connected inverter that applies a high frequency isolation transformer. Current sourcing at the output implies that, ideally, the injected current will be independent on the load voltage. The current injected to the line is controlled by varying the switching frequency and dithering at low currents. The system does not require the sensing of the output current or even the line voltage - except for synchronization. This is in contrast to the conventional voltage sourcing inverters where the small disturbance at the line voltage may lead to current run away and consequently a tight current feedback loop must be applied.**

The proposed topology and several proposed control approaches were analyzed and verified by simulations and by experiments. The simulation and experimental results confirm the theoretical analysis and show that the proposed inverter can be operated with no sensing of the line current or voltage.

I. INTRODUCTION

Grid connected inverters are important building blocks in renewable energy conversion systems. As described in earlier publications, they can be realized by a two stage topology [1, 2] or as a one stage system [3-5]. When isolation is required, it can be accomplished by introducing a line frequency transformer between the output filter and the grid utility [6]. Reduction of the physical size and cost of the inverter can be achieved by placing the isolation transformer at a high frequency branch as proposed in [7, 8]. A high frequency PWM non-isolated inverter that operates under soft-switching conditions was proposed in [9] while an isolated soft-switched inverter was shown in [10].

Notwithstanding the disparity of the many solutions proposed hitherto for grid connected inverters, most of them share a common feature - their outputs are basically voltage sources. Consequently, any mismatch between the synthesized output waveforms of these inverters and the grid voltage will generate large erroneous currents unless a current feedback is used to control the magnitude and phase of injected current.

An alternative approach to the grid connected inverter design, explored in this study, is to apply an inverter with an Output Current Sourcing (OCS) behavior rather than the voltage sourcing one*. Current sourcing at the output implies that, ideally, the injected current will be independent of the load voltage. Grid connected OCS inverters were presented in [11] applying a flyback converter and in [12] based on a series resonant converter followed by a diode rectifier and a polarity commutator. To exhibit the OCS characteristics the circuit in [12] must be operated below half the resonant frequency (discontinuous current conduction mode) and consequently, the reactive current in the resonant tank is expected to be high, especially at high power levels, and the resonant capacitor will have large physical dimensions.

This study describes an isolated OCS grid connected inverter that is based on the "AC inductor" concept described in [13]. “AC inductors” have several advantages over “DC inductors” [13]: (1) the current in “AC inductors” reverses its polarity every switching cycle making it easier to achieve soft switching, (2) the average low frequency component of the voltage across the “AC inductors” remains zero, reducing significantly the risk of a current run away and importantly, (3) “AC inductors” exhibit an OCS behavior and hence they are less sensitive to the output voltage waveform shape and distortion and to disturbances at either input or load side.

The proposed topology operates under soft switching conditions and does not require a resonant capacitor.

II. SYSTEM DESCRIPTION

The proposed inverter comprises two H bridges Q_1-Q_4 and Q_5-Q_8 (Fig. 1), a main inductor L_{in}, high frequency isolating transformer T1, and output rectifier D_1-D_4.

The input bridge, which operates under zero voltage switching conditions at turn on, generates a high frequency symmetrical square wave that is applied to the main inductor. The triangular current of the inductor is reflected to the secondary of the isolating transformer T1 and rectified by D_1-D_4. The rectified current is filtered by

* Note that by an Output Current Sourcing (OCS) inverter we mean here an inverter that behaves as a current source at it's output rather than a having a current source supply (i.e. an inductor between the input voltage and H bridge).

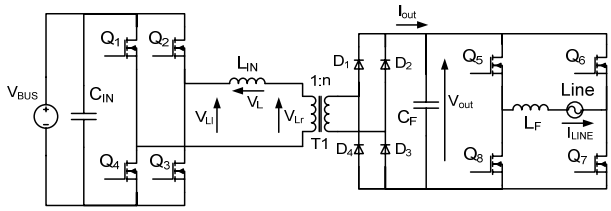

Fig. 1. The proposed grid connected inverter.

the output filter (C_F, L_F in Fig. 1) and fed to the line through the output bridge Q_5-Q_8 that is synchronized to the line and acts as a polarity commutator.

The theoretical analysis of the proposed inverter was carried out under the assumption that the switching frequency of the input bridge is much higher than the line cycle, and hence one can assume that the voltage V_{out} applied to the output rectifier, at every given time instant (t) of the line cycle, is practically constant. Consequently, the high frequency portion of the inverter can be analyzed by assuming that the output voltage is constant as was described in [13]. For the sake of brevity only the essentials of the analysis are repeated here.

During the time interval t_1-t_2 (Fig. 2) of the high frequency switching cycle, the peak inductor current Ipk is:

$$Ipk = \frac{V_{bus} - \frac{V_{out}}{n}}{L_{in}}(t_2 - t_1) \tag{1}$$

where Lin is the inductance of the inductor. Similarly, during the time interval t_2-t_3 Ipk is expressed as:

$$Ipk = \frac{V_{bus} + \frac{V_{out}}{n}}{L_{in}}(t_3 - t_2) \tag{2}$$

From (1) and (2), and taking into account that (t_3-t_1) is half a switching cycle:

$$(t_2 - t_1) + (t_3 - t_2) = I_{pk} L_{in} \frac{2V_{bus}}{V_{bus}^2 - \left(\frac{V_{out}}{n}\right)^2} = \frac{1}{2F} \tag{3}$$

where F is the switching frequency.

Rearranging (3) back for Ipk we get:

$$Ipk = \frac{V_{bus}^2 - \left(\frac{V_{out}}{n}\right)^2}{4L_{in}FV_{bus}} \tag{4}$$

The output current is the rectified current of the inductor (reflected to the secondary of the isolation transformer) as depicted in Fig. 3. Since the output current is of a triangular shape, its average value is half its peak value:

$$\bar{I}_{out} = \frac{1}{2}\frac{Ipk}{n} = \frac{V_{bus}^2 - \left(\frac{V_{out}}{n}\right)^2}{8nL_{in}FV_{bus}} \tag{5}$$

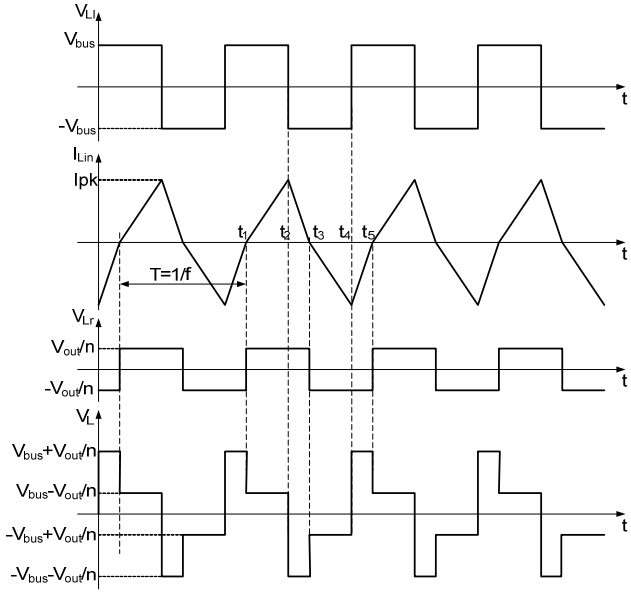

Fig. 2. Basic waveforms of the proposed inverter. From top to bottom: V_{L1}, Inductor current, V_{Lr}, voltage across inductor.

where $\bar{I}_{out}$ is the output current averaged over the switching cycle.

It is assumed that the line voltage, which absolute value equals to the output voltage, i.e. $V_{out}=|V_{line}(t)|$, is of form:

$$V_{line}(t) = V_{rms}\sqrt{2}\sin 2\pi f_{line} t \tag{6}$$

where V_{rms} is rms value of the line voltage, f_{line}- line frequency.

Considering (6), (5) can be rewritten as follows:

$$\bar{I}_{out}(t) = \frac{V_{bus}^2 - \frac{1}{n^2}V_{line}^2(t)}{8 \cdot n \cdot L_{in} \cdot F(t) \cdot V_{bus}} \tag{7}$$

where $\bar{I}_{out}(t)$ is the average output current of the inverter and F(t) is the switching frequency at time instant t.

Apparently, the energy will be delivered to the grid if and only if the nominator of (7) is positive. Consequently the lower limit for "n" will be given as follows:

$$n > \frac{V_{rms}\sqrt{2}}{V_{bus}} \tag{8}$$

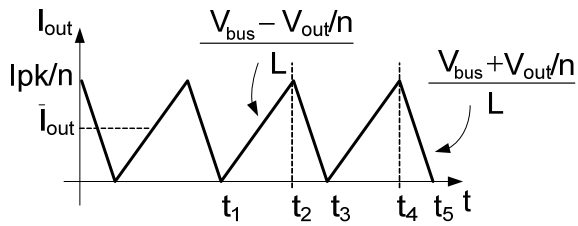

Fig. 3. Zoom on I_{out} (Fig. 1).

Since the goal of a grid connected inverter is to deliver a current which is in phase with, and of the shape of the line voltage, the inverters output current should be of form:

$$\bar{I}_{out}(t) = I_{rms}\sqrt{2}\sin 2\pi f_{line}t = \frac{P_{out}}{V_{rms}}\sqrt{2}\sin 2\pi f_{line}t \qquad (9)$$

Where I_{rms} is rms value of the line current, P_{out} – average power delivered to the line.

Considering (6), (9) can be rewritten as follows:

$$\bar{I}_{out}(t) = \frac{P_{out}V_{line}(t)}{V_{rms}^2} \qquad (10)$$

Equations (10) and (7) can now be used to obtain the expression for the switching frequency as a function of time F(t), that will ensure a sinusoidal current injection into the grid:

$$F(t) = K_p \frac{V_{bus}^2 - \frac{1}{n^2}V_{line}^2(t)}{V_{line}(t)},$$

$$\text{where } K_p = \frac{V_{rms}^2}{8nL_{in}P_{out}V_{bus}} \qquad (11)$$

Based on (11), three different control approaches can be considered. One option is to measure the instantaneous line voltage $V_{line}(t)$ and apply the sampled value to calculate the required frequency F(t) of the input bridge gate pulses according to (11). The coefficient K_p can be considered as a scaling factor that will be obtained from the Maximum Power Point Tracking (MPPT) algorithm. For any given operating conditions, K_p will be adjusted by the MPPT section to obtain the maximum power available from the photovoltaic cell panels.

Another option for deriving F(t) is to measure only the rms value of the line voltage (much lower sampling rate) and calculate the V_{line} according to (6). For this case, (11) can be rewritten as follows:

$$F(t) = K_p \frac{V_{bus}^2 - \frac{2}{n^2}V_{rms}^2\sin^2(2\pi f_{line}t)}{V_{rms}\sin(2\pi f_{line}t)} \qquad (12)$$

Yet another control option would be to calculate the frequency F(t) without sensing the line voltage at all. This can be accomplished by assuming some predefined (nominal) rms value of the line voltage (V_{nom}):

$$F(t) = K_p \frac{V_{bus}^2 - \frac{2}{n^2}V_{nom}^2\sin^2(2\pi f_{line}t)}{V_{nom}\sin(2\pi f_{line}t)} \qquad (13)$$

Although there is no need to measure the line voltage in this case, there would be a need to synchronize the operation to the line frequency by, for example, sensing the zero crossing of the line voltage.

It should be stressed though that none of the above mentioned control methods require the sensing of the output current.

From the practical point of view, the first approach is the most complicated one as it requires line sensing circuitry with rather high sampling rate. In the second case, the sampling rate can be much lower as only the rms value of the line voltage needs to be measured. However, the current injected to the line may be slightly distorted. The third method is the simplest among the suggested control approaches since no line sensing circuitry is needed except for synchronization. On the other hand, the THD of the current generated in this case will increase as the difference between the nominal and actual rms values of the line voltage increases.

By combining (7) and (13), the current generated in this case is found to be:

$$\bar{I}_{out}(t) = \frac{P_{out}}{V_{nom}^2}\frac{1-\alpha^2\beta^2\sin^2(2\pi f_{line}t)}{1-\beta^2\sin^2(2\pi f_{line}t)}V_{nom}(t) \qquad (14)$$

where:

$$V_{nom}(t) = V_{nom}\sqrt{2}\sin(2\pi f_{line}t),\ \alpha = \frac{V_{rms}}{V_{nom}},\ \beta = \frac{\sqrt{2}}{n}\frac{V_{nom}}{V_{bus}}.$$

It is evident from (14) that the current is, theoretically, sinusoidal if the rms value of the line voltage is equal to the predefined value V_{nom} ($\alpha = 1$). The line current distortion will increase as the line voltage deviates from the nominal value. It follows from (14) that the lower the β the lower the distortion is. That is, for the given line and bus voltages it is advantageous (from the distortion point of view) to choose as high “n” as possible. It should be noted though, that the rms current of the primary increases as "n" goes up. Hence, there is a tradeoff between THD and loss reduction.

Choosing “n” values close to its lower limit (eq. 8) will guarantee the lowest possible inductance of the main inductor (assuming the same switching frequency at the peak of the line voltage), which can help to use the leakage inductance of the isolation transformer as a main inductor. The downside of a small "n" will be, as pointed out above, a higher THD in the case of line voltage variations. Another shortcoming of a small “n” is a wider switching frequency range over the line cycle. That is, for the same switching frequency at the line voltage peak, the design with a smaller "n" will require higher switching frequencies at low line voltages.

This can be demonstrated by calculating the ratio of the relative change of F(t) per relative line voltage change, CG, that is required to shape the current injected into the grid:

$$CG = \frac{\frac{\partial F(t)}{F(t))}}{\frac{\partial V_{line}(t)}{V_{line}(t)}} = \frac{\partial F(t)}{\partial V_{line}(t)}\frac{V_{line}(t)}{F(t)} \qquad (15)$$

where F(t) is given in (11).

Taking the derivative of (11) with respect to V_{line} and substituting it back into (15) yields:

$$CG = -\frac{n^2\gamma^2+1}{n^2\gamma^2-1} = -1 - \frac{2}{n^2\gamma^2-1} \qquad (16)$$

where $\gamma = \frac{V_{line}(t)}{V_{bus}}$.

Equation (16) shows that when "n" is close to its lower limit (8), the denominator of (16) approaches zero, so CG is very high. In this case the rate of frequency change required to shape the current injected into the line, will be higher. This means that a smaller “n” will require a larger overall frequency changes from peak line voltage to the low line voltages.

In all three alternatives (11-13) the frequency needs to go to high (and even impractical) values around the zero crossing of the line voltage when its voltage levels, and hence the current levels, are low. One possible approach to overcome this practical limitation is to limit the drive frequency to some maximum value F_{lim} and to apply dithering. That is, periods of global 'on' and 'off' sequences of the drive at a lower modulating frequency. Namely, to skip switching cycles so as to obtain the required average value of the output current. The required global duty cycle will thus be:

$$D_G(t) = \frac{F_{\lim}}{F(t)} \qquad (17)$$

where F(t) is the frequency calculated according to (11-13).

The effect of the switching cycle skipping on the output current is demonstrated in Fig. 4.

Another way to avoid going to high frequencies is to apply pulse width modulation while staying at constant switching frequency. In this mode of operation, two diagonal switches (say Q1 and Q3) are kept "on" for some time interval t_{on}, allowing the inductor's current to increase (Fig. 5a), and then switched "off". During "t_{off}" the current keeps flowing in the same direction and hence the body diodes of Q2 and Q4 will conduct until the current through the inductor reaches zero. In the next switching cycle, the sequence is repeated for Q2, Q4 and body diodes of Q1, Q2. The output current which is the rectified current of the inductor is shown in Fig. 5b.

The average of the output current over the switching cycle is given as:

$$\bar{I}_{out}(t) = \frac{1}{n}\left[\frac{V_{bus}-\frac{V_{out}}{n}}{L}t_{on}^2 + \frac{V_{bus}+\frac{V_{out}}{n}}{L}t_{off}^2\right] f_{DCM} \qquad (18)$$

where $f_{DCM} = 1/T_{DCM}$

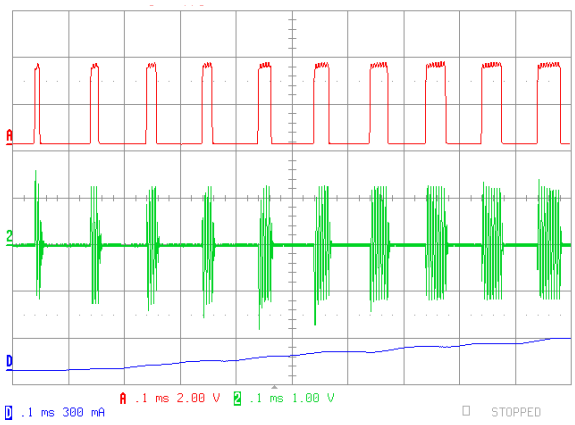

Fig. 4. Dithering mode around zero cross.
Upper trace: modulating carrier; middle trace: inductor's current; lower trace: filtered output current.

From Fig. 5a, the ratio of "t_{on}" to "t_{off}" can be expressed as:

$$\frac{t_{off}}{t_{on}} = \frac{V_{bus}-\frac{V_{out}}{n}}{V_{bus}+\frac{V_{out}}{n}} \qquad (19)$$

Substituting this back to (18) yields:

$$\bar{I}_{out}(t) = \frac{2V_{bus}\cdot t_{on}^2}{nL}\frac{V_{bus}-\frac{V_{out}}{n}}{V_{bus}+\frac{V_{out}}{n}} f_{DCM} \qquad (20)$$

For the output current to follow the line voltage, (20) should be equal to (10). Since $|V_{out}|=|V_{line}(t)|$, "t_{on}" can be expressed as:

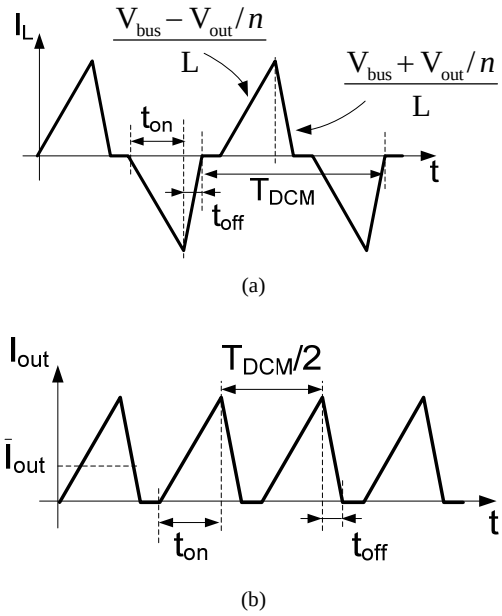

Fig. 5. PWM mode of operation.
(a) Inductor's current; (b) output current.

$$t_{on} = \sqrt{\frac{P_{out} V_{line}(t) Ln}{2V_{rms}^2 V_{bus} f_{DCM}} \frac{V_{bus} + \frac{1}{n} V_{line}(t)}{V_{bus} - \frac{1}{n} V_{line}(t)}} \qquad (21)$$

The main advantage of the dithering method is its simplicity. However, the low frequencies components resulted by the dithering will call for stronger filter at the input of the inverter. In addition, the "resolution" of the global duty cycle D_G (eq. 17) is rather limited since F_{lim} and F(t) are relatively close to each other.

The PWM method has higher accuracy as compared to the dithering method, but may produce fairly high currents in the inductor. Moreover, if sensing of the output voltage is considered, it consumes much more computing resources in order to calculate "t_{on}" (eq. 21).

III. Simulation Results

The control methodologies described above were verified by a cycle-by-cycle simulations as well as by a behavioral simulation model of the proposed current sourcing inverter.

A. Behavioral Simulation Model

The behavioral simulation model (Fig. 6) of the proposed inverter is based on the "AC inductor" behavioral model described in [13].

The main difference between this model and the one given in [13] is that the output voltage is represented here by the sinusoidal voltage source (E3) rather than by the constant voltage source as in [13]. The behavioral source ABM13 generates the frequencies according to (11-13). Parameter "alpha" corresponds to "α" in (14).

For the simulation according to control methods described by (11) and (12), "alpha" is chosen to be unity. For the case described by (13), "alpha" is set according to the expected ratio between the nominal and the actual rms value of the utility. Fig. 7 shows the simulated inductor's current for the cases when the line voltage is equal to its nominal value and when the difference between the nominal and the line voltages is $\pm 5\%$. The power factor of the simulated output current when the line voltage is within 10% of the nominal voltage is presented in Fig. 8. The power was set to about 1kW, and the input voltage (V_{bus}) was 400V.

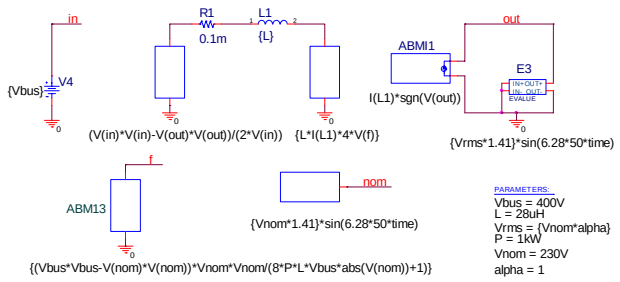

Fig. 6. Behavioral simulation model of the proposed inverter.

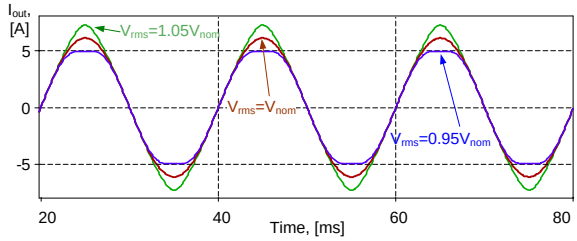

Fig. 7. Simulated output current for different line voltages.

B. Cycle-by-Cycle Simulation Model

Cycle-by-cycle simulation was performed on a power electronics simulator (PSIM, version 7.1; Powersim, USA). The simulation model (Fig. 9) comprised the power stage (input HF bridge M1-M4, diode rectifier D1-D4, and power inductor L1). The rectified line voltage at the output is emulated by the dependent sources (Vline, Fline). The frequency is generated according to (11) by a computation block F5. The output voltage is sensed by the voltage sensor VSEN1. IFblock is responsible for switching from the 50% square wave to PWM modulation when the switching frequency goes above 200kHz. Once this limit is reached, the input bridge is switched at a constant frequency of 200kHz and "t_{on}" is generated according to (21) by the computation block F7.

The simulated inverter is fed from the "PV panel" behavioral block that models the behavior of the photovoltaic panel (Fig. 10).

The relationship between the output current and the output voltage of the "Cells" block was set to:

$$I_C = I_S - 10^{-8}\left(e^{\frac{V_C}{k \cdot 26 \cdot 10^{-3}}} - 1\right) \qquad (22)$$

where I_C is output current of the "Cells" block, V_C its output voltage and I_S is a variable that emulates the (linear) dependence of the output characteristic of the "PV panel" on the insolation levels. The constant 'k' determines the number of cells in the "PV panel" and it was set to 1000.

Fig. 11 shows the output characteristics of the "PV panel" block at two different insolation levels (I_S=2.5A, 3.65A) that correspond to a maximum power of 1kW and 1.5kW respectively. The simulation results for these two operating conditions are presented in Fig. 12.

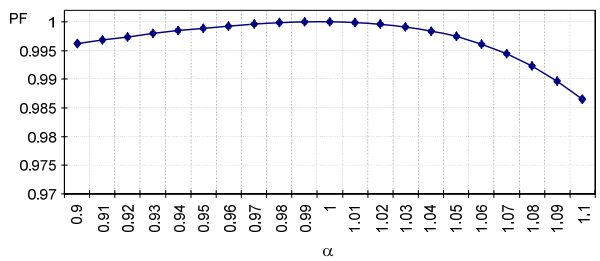

Fig. 8. PF of the simulated output current versus "α" (without measuring the output voltage).

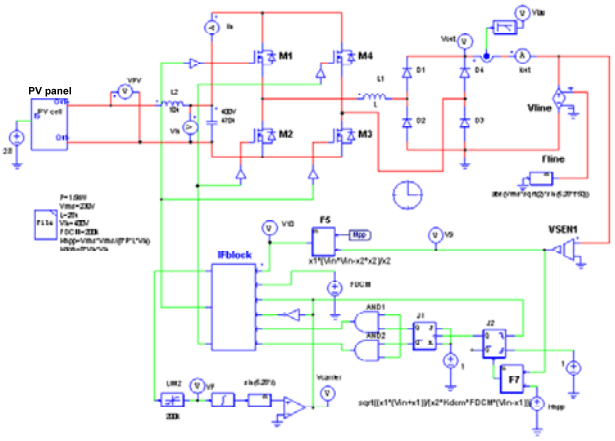

Fig. 9. PSIM cycle-by-cycle simulation model.

IV. Experimental

The behavior of the proposed "AC inductor" based OCS inverter was tested experimentally on a 3.5kW prototype that was build according to the topology shown in Fig. 1 and was powered by a DC voltage source. The transformer ratio "n" was set to 1. The value of the main inductor was 28µH. The switching frequency varied from 30kHz at the maximum of the line voltage up to 200kHz. Near the zero crossings of the line voltage, the switching cycles of the input bridge were dithered to obtain sinusoidal shaped average current while staying at the constant switching frequency of 200kHz.

The circuit was controlled by a DSP (320F2808, TI). Tests were run up to a power level of 1kW.

Fig. 13 shows the output current measured when the inverter's output voltage was set to 110Vrms. The THD was 3%. Fig. 14 presents the current obtained for the case when the output of the inverter was shorted. In both cases the switching frequency was generated according to (13) assuming a V_{nom} value of 110V.

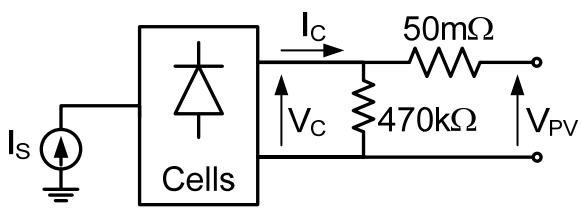

Fig. 10. "PV panel" block model.

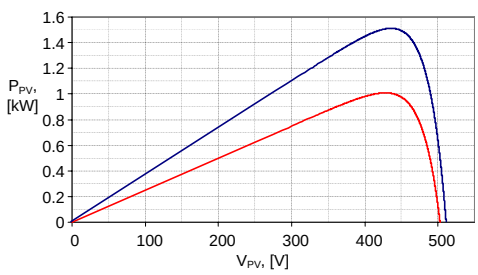

Fig. 11. Output power of "PV panel" block used in cycle-by-cycle simulation.

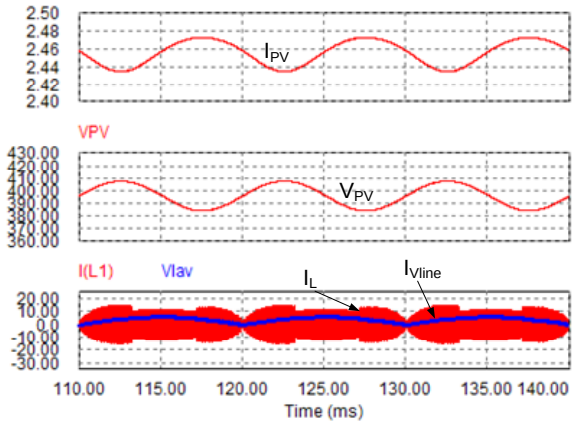

(a)

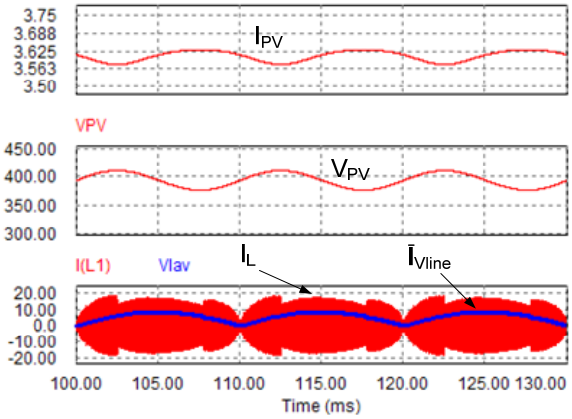

(b)

Fig. 12. Cycle-by-cycle model simulation results.
(a) at max. power point of 1kW; (b) at max. power point of 1.5kW.

V. Discussion and Conclusions

This study presents an "AC inductor" based OCS inverter that is controlled by varying the switching frequency. All the switches are switched under zero voltage at turn on.

It is evident from (7) that the current injected into the line is not independent of the line voltage. It was shown, however, that the influence of the line voltage on the output current can be reduced considerably by proper design. Consequently, the proposed topology behaves as a current source for all practical needs.

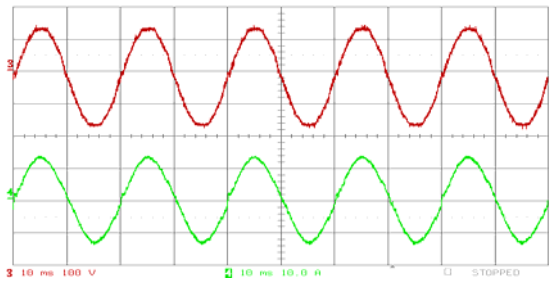

Fig. 13. Output behavior of the inverter with no sensing of the output voltage. Vin=318V; Vline=110Vrms; Pout=1kW.
Upper trace: output voltage 100V/div; Lower trace: line current (I_{LINE}) 10A/div; Horizontal scale: 10ms/div.

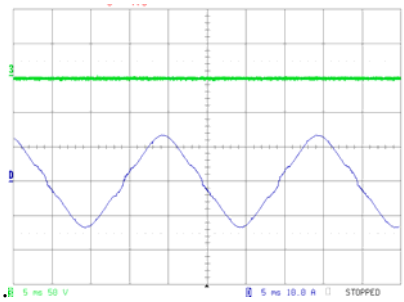

Fig. 14. Output current of the inverter with shorted output. Vin=265V; Upper trace: output voltage (shorted); Lower trace: line current (I_{LINE}) 10A/div; Horizontal scale: 5ms/div.

Simulations and experimental results verify the theoretical predictions that the proposed control method, with no sensing of the line voltage, makes the inverter act as a stable current source. In this control method the obtained current shape might become distorted if the difference between the actual and assumed nominal rms values of the line voltage is significant. However, due to the OCS capabilities of the proposed inverter, the generated output current was very close to the nominal sinusoid shape even when the output was shorted (Fig. 14)

The simulation and experimental results show that the proposed inverter can be operated in open loop, i.e. with no need to sense the line current and even without sensing the line voltage – except for synchronization. This is in contrast to the conventional voltage sourcing inverters where even a small disturbance at the line voltage may lead to current run away and consequently a tight current feedback loop must be applied.

REFERENCES

[1] F. Huang, G. Zhimin, T. Forughian, and D. Tien, "A new microcontroller based solar energy conversion modular unit," *Power Conversion Conference - Nagaoka 1997., vol. 2, pp. 697-700, 3-6 Aug. 1997.*

[2] K. Chomsuwan, P. Prisuwanna, and V. Monyakul, "Photovoltaic grid-connected inverter using two-switch buck-boost converter," *Twenty-Ninth IEEE Photovoltaic Specialists Conference, 2002, pp. 1527 – 1530, 19-24 May 2002.*

[3] Z. Chunjiang, C. Lingling, G. Herong, Z. Yanping, and W. Weiyang "Grid-connected inverters interface control with unified constant-frequency integration control," *Eighth International Conference on Electrical Machines and Systems, ICEMS 2005, vol. 2, pp. 982–985, 27-29 Sept. 2005.*

[4] Y. Chen and K. M. Smedley, "A cost-effective single-stage inverter with maximum power point tracking," *IEEE Transactions on Power Electronics, issue 5, vol. 19, pp. 1289-1294, Sept. 2004.*

[5] K. Hirachi, M. Ishitobi, K. Matsumoto, H. Hattori, M. Ishibashi, M. Nakaoka, N. Takahashi, and Y. Kato, "Pulse area modulation control implementation for single-phase current source-fed inverter for solar photovoltaic power conditioner," *1998 International Conference on Power Electronic Drives and Energy Systems for Industrial Growth 1998, vol. 2, pp. 677-682, 1-3 Dec. 1998.*

[6] Mihai Ciobotaru, Remus Teodorescu and Frede Blaabjerg, "Control of single-stage single-phase PV inverter," *European Conference on Power Electronics and Applications 2005, pp. 1-10, 11-14 Sept. 2005.*

[7] D. C. Martins and R. Demonti, "Interconnection of a photovoltaic panels array to a single-phase utility line from a static conversion system," *IEEE 31st Annual Power Electronics Specialists Conference, PESC 00, vol 3, pp. 1207 – 1211, 18-23 June 2000.*

[8] T. Takebayashi, H. Nakata, M. Eguchi, and H. Kodama, "New current feedback control method for solar energy inverter using digital signal processor," *Power Conversion Conference - Nagaoka 1997, vol. 2, pp. 687–690, 3-6 Aug. 1997.*

[9] S. Saha, N. Matsui, and V. P. Sundarsingh, "Design of a low power utility interactive photovoltaic inverter," 1998 International Conference on Power Electronic Drives and Energy Systems for Industrial Growth, 1998, vol 1, pp. 481–487, 1-3 Dec. 1998.

[10] D. A. Torrey, S. Kittiratsatcha, T. B. Bashaw, and R. T. Carpenter, "Inverter topology for utility-interactive distributed generation sources," *U. S. Patent 2005/0180175 A1, August 18, 2005.*

[11] A. C. Kyritsis, N. P. Papanikolaou, E. C. Tatakis, and J. C. Kobougias, "Design and control of a current source flyback inverter for decentralized grid connected photovoltaic systems," *European Conference on Power Electronics and Applications, 2005, pp. 1-10, 11-14 Sept. 2005.*

[12] K. Al-Haddad, R. Chaffai, and Rajagopalan, "High frequency inverter using zero current turn off COMFET switches for solar energy conversion," *12th International Telecommunications Energy Conference, INTELEC '90, pp. 41-46, 21-25 Oct. 1990.*

[13] I. Zeltser and S. Ben-Yaakov, "Modeling, analysis and simulation of "AC inductor" based converters," *Power Electronics Specialists Conference 2007, PESC 2007, pp. 2128 – 2134, 17-21 June 2007.*